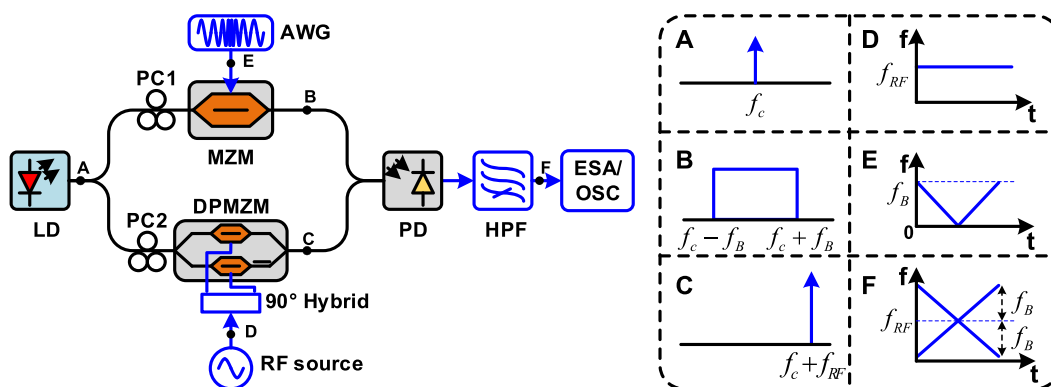# Photonics-Assisted Bandwidth-Doubling Dual-Chirp Microwave Signal Generation With Freely-Tunable Central Frequency

Lingjie Zhang
Zhen Zeng
Yaowen Zhang
Zhiyao Zhang
Bao Sun
Shangjian Zhang
Yali Zhang
Yong Liu

Photonics-Assisted Bandwidth-Doubling Dual-Chirp Microwave Signal Generation With Freely-Tunable Central Frequency

Lingjie Zhang [ID] **, Zhen Zeng, Yaowen Zhang, Zhiyao Zhang** [ID] **, Bao Sun, Shangjian Zhang** [ID] **, Yali Zhang, and Yong Liu**

State Key Laboratory of Electronic Thin Films and Integrated Devices, School of Optoelectronic Science and Engineering, University of Electronic Science and Technology of China, Chengdu 610054, China

Abstract: A photonics-assisted dual-chirp microwave signal generation scheme is proposed based on electro-optic modulation and heterodyne detection. The dual-chirp microwave signal is generated by heterodyne beating between a dual-chirp optical waveform and a frequency-shifted optical carrier, where the dual-chirp optical waveform is obtained by applying a baseband symmetric-triangle linear frequency modulated signal to a Mach-Zehnder modulator biased at the minimum transmission point, and the frequency-shifted optical carrier is obtained by carrier-suppressed single-sideband modulation in a dual-parallel Mach-Zehnder modulator (DPMZM) with the assistance of an electronic 90° hybrid. The bandwidth of the generated dual-chirp microwave signal is twice of that of the input baseband signal, and the central frequency can be tuned by varying the frequency of the single-tone microwave signal applied to the DPMZM. Both numerical simulation and experiment are carried out to demonstrate the proposed scheme. In the simulation, a dual-chirp microwave signal with a center frequency of 15 GHz and a bandwidth of 6 GHz is generated. In the proof-of-concept experiment, dual-chirp microwave signals centered at 1.5 GHz and with bandwidth of 100 MHz and 200 MHz are generated, which verifies the feasibility of the proposed scheme.

Index Terms: Dual-chirp microwave signal, pulse compression, matched filtering, range-Doppler coupling effect.

1. Introduction

In modern radar systems, linearly chirped microwave signals are widely employed to enhance the range resolution through pulse compression technology [1], [2]. Nevertheless, for a fast-moving target, an additional time shift of the compressed pulse is induced by the Doppler frequency shift, which introduces a measurement ambiguity of the target location [3]. This phenomenon is known as range-Doppler coupling effect, which can be effectively suppressed by using a dual-chirp microwave signal involving a pair of complementary linearly-chirped waveforms in the same time duration. The Doppler-frequency-shift-induced time increments for the up-chirped waveform and the down-chirped one are inverse to each other. Therefore, the range-Doppler coupling effect can be canceled out by averaging the arrival times of two waveforms in the same echo signal [4], [5].

The most common method of generating a dual-chirp microwave signal is using a direct digital synthesizer (DDS). However, the central frequency and the bandwidth of the generated signal are limited to multi-GHz due to the relatively low sampling rate of the digital-to-analog converter (DAC) available in the DDS [6], [7]. In order to overcome this limitation confronted by electronic approach, several photonics-assisted dual-chirp microwave signal generation schemes have been proposed in recent years due to the prominent advantages of photonic technology such as ultra-broad bandwidth and immunity to electromagnetic interferences [8]–[18]. A photonics-assisted dual-chirp microwave signal generation scheme was first proposed and demonstrated based on a single dual-parallel Mach-Zehnder modulator (DPMZM) [10]. In this scheme, a baseband single-chirp waveform and a single-tone radio-frequency (RF) signal are separately applied to the two sub-MZM in the DPMZM, where both of the sub-MZMs are biased at the minimum transmission point to achieve carrier-suppressed double-sideband (CS-DSB) modulation. After photodetection (PD), a dual-chirp microwave signal with its chirp rate and duration (i.e., bandwidth) identical to those of the baseband single-chirp waveform and its central frequency identical to the single-tone RF signal, is generated through heterodyne beat between the modulation sidebands. In order to enhance the operation frequency and bandwidth, schemes based on two cascaded MZMs have been proposed [11], [12]. In [11], a single-tone RF signal with a frequency of f_1 is applied to the first MZM biased at the minimum transmission point, and a single-chirp waveform with a central frequency of f_2 is applied to the second MZM biased at the maximum transmission point. Through setting $f_1 = 4f_2$, a dual-chirp microwave signal with its central frequency equal to f_1 and a quadrupling-bandwidth of the input single-chirp waveform is generated after photodetection. Other approaches to generating a frequency- and bandwidth-multiplied dual-chirp microwave signal have also been demonstrated based on various polarization multiplexed electro-optic modulators such as a dual-polarization quadrature phase shift keying (DP-QPSK) modulator [13]–[15] and a dual-polarization binary phase shift keying (DP-BPSK) modulator [16], [17]. Another approach to generating a dual-chirp microwave signal is based on Fourier domain mode-locking (FDML) optoelectronic oscillator (OEO) [18]. In the OEO cavity, an opposite frequency-scanning dual-passband microwave photonic filter (MPF) is constructed based on phase-to-intensity modulation conversion by using an optical notch filter and two laser diodes driven by triangle current. Through setting the cavity round-trip time equal to multiples of the frequency-scanning period, a dual-chirp microwave signal will oscillate in the OEO loop based on FDML operation. The limitation of using an FDML OEO to generate a dual-chirp microwave signal lies in the following aspects. Firstly, it can only generate a continuously and periodically varying waveform with a maximum period equal to the cavity round-trip time (generally below tens of microsecond), which puts a limitation to the measurement range of the radar system due to the relatively small duration. Secondly, the frequency-scanning linearity is generally poor, which will degrade the range resolution of the radar system. Thirdly, mode competition may induce failure of simultaneous dual-frequency oscillation in the cavity if the net gain is not flat in the desired frequency range. Comparing with the FDML OEO scheme, electro-optic modulation is a more flexible and simple method to realize dual-chirp microwave signal generation.

In this paper, a bandwidth-doubling and frequency-tunable dual-chirp microwave signal generation scheme is demonstrated based on electro-optic modulation and heterodyne detection. In the proposed scheme, a baseband single-chirp waveform is applied to the MZM biased at the minimum transmission point to generate a dual-chirp optical waveform. After heterodyne beating with a frequency-shifted optical carrier from a DPMZM driven by a tunable single-tone RF signal via an electrical 90° hybrid, a dual-chirp microwave signal with double-bandwidth of the input baseband single-chirp waveform is generated, whose central frequency is equal to the input single-tone RF signal. Both simulation and experiment are carried out to demonstrate the feasibility of the proposed scheme. Besides, the pulse compression ratio is also investigated.

2. Operation Principle

Fig. 1 shows the schematic diagram of the proposed photonics-assisted dual-chirp microwave signal generation. Continuous-wave (CW) light at f_c from a laser diode (LD) is divided into
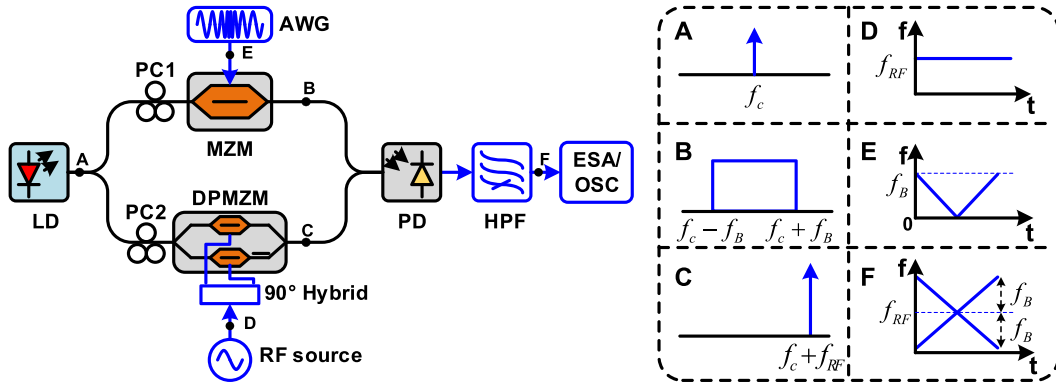
Fig. 1. Schematic diagram of the proposed dual-chirp microwave signal generation. LD: laser diode; PC: polarization controller; AWG: arbitrary waveform generator; MZM: Mach-Zehnder modulator; DP-MZM: dual-parallel Mach-Zehnder modulator; PD: photodetector; HPF: high-pass filter; ESA: electronic spectrum analyzer; OSC: oscilloscope. In the dashed box, the spectra at points A, B and C are shown in the left column, and the frequency-time diagrams of the microwave signals at point D, E and F are presented in the right column.

two branches by a 3-dB optical coupler. In the upper branch, the CW light is modulated by a specially-set baseband signal from an arbitrary waveform generator (AWG) via an MZM biased at the minimum transmission point. The baseband signal is a symmetric-triangle linear frequency modulated (LFM) signal with a bandwidth of f_B, whose frequency-time diagram is shown in the dashed box (point E) in Fig. 1. In the first half of the duration, the frequency of the baseband signal decreases linearly from f_B to direct current (DC), while in the second half of the duration, it increases from DC to f_B. After CS-DSB modulation, the optical carrier is suppressed, and the frequency of the $\pm$1st-order modulated sideband varies from $f_c \pm f_B$ to f_c in the first half of the duration, while in the second half of the duration it varies from f_c to $f_c \pm f_B$. Hence, a dual-chirp optical waveform with frequencies linearly sweeping from $f_c \pm f_B$ to $f_c \mp f_B$ is generated, whose spectrum is presented in the dashed box (point B) in Fig. 1. In the lower branch, the CW light is shifted in the frequency domain via an electro-optic frequency shifter which is composed of a DPMZM and an electronic 90° hybrid. The DPMZM consists of a parent MZM (p-MZM) biased at its quadrature point and two sub-MZMs biased at their minimum transmission point, which works at carrier-suppressed single-sideband (CS-SSB) modulation mode with assistance of the electronic 90° hybrid. Through applying a single-tone RF signal with a frequency of f_{RF} ($f_{RF} > f_B$) to the CW light via the frequency shifter, a frequency-shifted optical carrier centered at $f_c + f_{RF}$ (or $f_c - f_{RF}$) is generated, where the frequency-upshifted/downshifted optical carrier can be switched by exchanging the bias voltage of the p-MZM between two quadrature points at the rising and falling edge of the transmission curve. After combining the two optical signals for heterodyne detection in a photodetector, a dual-chirp microwave signal with frequencies linearly sweeping from $f_{RF} \pm f_B$ to $f_{RF} \mp f_B$ is generated, whose frequency-time diagram is shown in the dashed box (point F) in Fig. 1. Therefore, the bandwidth of the generated dual-chirp microwave signal is twice of that of the baseband signal applied to the upper branch, and the central frequency can be flexibly tuned by varying the frequency of single-tone RF signal applied to the lower branch. The high-pass filter (HPF) after the photodetector is used to filter out the generated baseband signal through beating between the two modulation sidebands of the optical signal from the upper branch.

Mathematically, in the upper branch, the output optical field from the MZM working in CS-DSB modulation state can be written as [19]

$$E_{MZM} = \frac{\sqrt{2}}{2} E_{in} \cos\left[m_{baseband} s(t) + \pi/2 \right] = -\frac{\sqrt{2}}{2} E_{in} \sin\left[m_{baseband} s(t) \right], \quad (1)$$

where E_{in} is the output optical field of the LD. $m_{baseband} = \pi V / V_{\pi}$ is the modulation index for the symmetric-triangle LFM signal $Vs(t)$, and V_{π} is the half-wave voltage of the MZM. The baseband symmetric-triangle LFM signal is expressed as

$$s(t) = \begin{cases} \cos\left(2\pi f_B t - \pi k t^2\right), 0 < t \leq \frac{T_d}{2} \\ \cos\left[\pi k \left(t - \frac{T_d}{2}\right)^2\right], \frac{T_d}{2} < t \leq T_d \end{cases}, \qquad (2)$$

where f_B and T_d are the bandwidth and the duration of the symmetric-triangle LFM signal, respectively. k is the chirp rate of $s(t)$, which can be calculated by $k = 2f_B / T_d$. Hence, the output optical field from the MZM can be written through using Jacobi-Anger expansion as

$$E_{MZM} = \begin{cases} \sqrt{2}E_{in} \sum_{n=1}^{\infty} (-1)^n J_{2n-1}(m_{baseband}) \cos\left[(2n-1)\left(2\pi f_B t - \pi k t^2\right)\right], 0 < t \leq \frac{T_d}{2} \\ \sqrt{2}E_{in} \sum_{n=1}^{\infty} (-1)^n J_{2n-1}(m_{baseband}) \cos\left[(2n-1)\pi k \left(t - \frac{T_d}{2}\right)^2\right], \frac{T_d}{2} < t \leq T_d \end{cases}, \qquad (3)$$

where $J_n(x)$ is the nth-order Bessel function of the first kind. In small-signal modulation, the higher-order harmonics can be neglected. Hence, Eq. (3) can be simplified as

$$E_{MZM} \approx \begin{cases} -\sqrt{2}E_{in} J_1(m_{baseband}) \cos\left(2\pi f_B t - \pi k t^2\right), 0 < t \leq \frac{T_d}{2} \\ -\sqrt{2}E_{in} J_1(m_{baseband}) \cos\left[\pi k \left(t - \frac{T_d}{2}\right)^2\right], \frac{T_d}{2} < t \leq T_d \end{cases}, \qquad (4)$$

In the lower branch, the output optical field from the DPMZM working in CS-SSB modulation state can be written as

$$E_{DPMZM} = \frac{\sqrt{2}}{4} E_{in} \cos\left[m_{RF} \cos(\omega_{RF} t) + \pi/2\right] e^{j\varphi_3/2} + \frac{\sqrt{2}}{4} E_{in} \cos\left[m_{RF} \sin(\omega_{RF} t) + \pi/2\right] e^{-j\varphi_3/2}, \qquad (5)$$

where m_{RF} is the modulation index for the RF signal ($\omega_{RF} = 2\pi f_{RF}$) applied to the DPMZM via a 90° hybrid. φ_3 is the bias phase difference between the two arms of the p-MZM in the DPMZM. Through exchanging $\varphi_3 = \pm \pi/2$, frequency-upshifted/downshifted optical carrier can be generated. In small-signal modulation, through using Jacobi-Anger expansion, the optical field of the frequency-upshifted optical carrier can be expressed as

$$E_{DPMZM} \approx -j\frac{\sqrt{2}}{2} E_{in} J_1(m_{RF}) e^{-j\omega_{RF} t - j\frac{\pi}{4}}, \qquad (6)$$

Therefore, the optical field injected into the PD is calculated by

$$E = \frac{\sqrt{2}}{2}(E_{MZM} + E_{DPMZM}), \qquad (7)$$

After photodetection, the output current can be calculated by

$$i(t) \propto EE^*, \qquad (8)$$

Through substituting Eq. (4) and Eq. (6) into Eqs. (7)-(8), the output current from the PD in small signal modulation situation is

$$i(t) \propto \begin{cases} E_{in}^2 J_1(m_{RF}) J_1(m_{baseband}) \left\{ \sin\left[2\pi (f_{RF} + f_B) t - \pi k t^2 + \frac{\pi}{4}\right] \right. \\ \left. + \sin\left[2\pi (f_{RF} - f_B) t + \pi k t^2 + \frac{\pi}{4}\right] \right\}, 0 < t \leq \frac{T_d}{2} \\ E_{in}^2 J_1(m_{RF}) J_1(m_{baseband}) \left\{ \sin\left[2\pi f_{RF} t - \pi k \left(t - \frac{T_d}{2}\right)^2 + \frac{\pi}{4}\right] \right. \\ \left. + \sin\left[2\pi f_{RF} t + \pi k \left(t - \frac{T_d}{2}\right)^2 + \frac{\pi}{4}\right] \right\}, \frac{T_d}{2} < t \leq T_d \end{cases}, \qquad (9)$$

It can be seen from Eq. (9) that a dual-chirp signal centered at f_{RF} is generated, whose bandwidth is $2f_B$. In the generated dual-chirp microwave signal, the up-chirped signal sweeps from $f_{RF} - f_B$

to $f_{RF} + f_B$, and the down-chirped one sweeps from $f_{RF} + f_B$ to $f_{RF} - f_B$. In addition, an identical dual-chirp microwave signal can also be generated when the frequency-downshifted optical carrier from the DPMZM is used.

3. Simulation Results

Simulation is implemented based on Eqs. (1), (2), (5), (7) and (8) in MATLAB to verify the feasibility of the proposed scheme to generate a dual-chirp microwave signal. In the simulation, the CW light from the LD has a wavelength of 1550 nm and a power of 16 dBm. The half-wave voltages of the MZM and the two sub-MZMs in the DPMZM are set to be 3 V. The frequency and the power of the single-tone RF signal applied to the lower branch are set to be 15 GHz and 8 dBm, respectively. The input baseband signal is a symmetric-triangle linear frequency modulated pulse signal with a peak-to-peak voltage of 0.5 V, an instantaneous bandwidth of 3 GHz and a duration of 0.8192 μs, which corresponds to a chirp rate of 7.324 GHz/μs. Fig. 2(a) and (b) show the waveform and the frequency-time diagram of the input baseband signal, respectively. Fig. 2(c) exhibits the generated dual-chirp microwave signal after photodetection. It can be seen from Fig. 2(c) that the expected dual-chirp microwave signal centered at 15 GHz is generated. Nevertheless, there is another dual-chirp signal in the baseband, which is attributed to the direct beating between the two modulation sidebands of the optical signal from the MZM, and can be filtered out by an HPF. Fig. 2(d) shows the output spectrum after a 4th-order Butterworth HPF with a cut-off frequency of 9 GHz. Fig. 2(e) and (f) present the waveform and the frequency-time diagram of the generated dual-chirp microwave signal centered at 15 GHz, respectively. It can be seen from Fig. 2(f) that a dual-chirp microwave signal with an instantaneous bandwidth of 6 GHz and a central frequency of 15 GHz is generated, in which the up-chirped and down-chirped components are in the same duration.

In order to exhibit the ability of the generated dual-chirp microwave signal to eliminate the range-Doppler coupling effect, pulse compression based on matched filtering is numerically implemented for the echo signals with and without a Doppler frequency shift. Fig. 3(a) and (b) shows the matched filtering results of the dual-chirp microwave signal without a Doppler frequency shift and with a Doppler frequency shift of 200 MHz, respectively, where the time delay of the echo signal is set to be 0 ns. It can be seen from Fig. 3(a) that there is a single peak located at 0 ns after pulse compression, which fits in with the time delay of the echo signal. Nevertheless, there are two peaks located at 27.3 ns and -27.3 ns in Fig. 3(b), respectively. The additional time delay of ±27.3 ns corresponds to the Doppler frequency shift of 200 MHz divided by the chirp rates of ±7.324 GHz/μs. Therefore, the range-Doppler coupling effect can be canceled out by averaging the arrival times of two peaks. In addition, it can be seen from the inset in Fig. 3(b) that the full-width at half maximum (FWHM) of the compressed pulse is about 0.2 ns, which corresponds to a pulse compression ratio of 4096. The pulse compression ratio is close to the time-bandwidth production (TBWP) of 4915. In theory, the compression ratio for an LFM signal with an even amplitude is generally lower than its TBWP. For example, as reported in [15], the pulse compression ratios were measured to be 171 and 341, where the corresponding TBWP are 204.8 and 409.6, respectively. In [20], the measured pulse compression ratio is 80800, which is also smaller than the TBWP of 88880.

4. Experiment Results and Discussion

In this section, a proof-of-concept experiment is carried out based on Fig. 1. The CW light at 1550 nm and with a power of 13 dBm is generated by a tunable optical source (Santec TSL-510), which is then divided into two branches by a 3-dB optical coupler. In the upper branch, the CW light propagates through a 10-Gbps MZM (T·DKH1.5-10PD-ADC) biased at the minimum transmission point, and is modulated by a baseband symmetric-triangle linear frequency modulated signal generated by a programmable AWG (RIGOL DG5352). In the lower branch, the CW light is CS-SSB modulated through a 40-Gbps DPMZM (COVEGA Mach-40086) driven by a single-tone
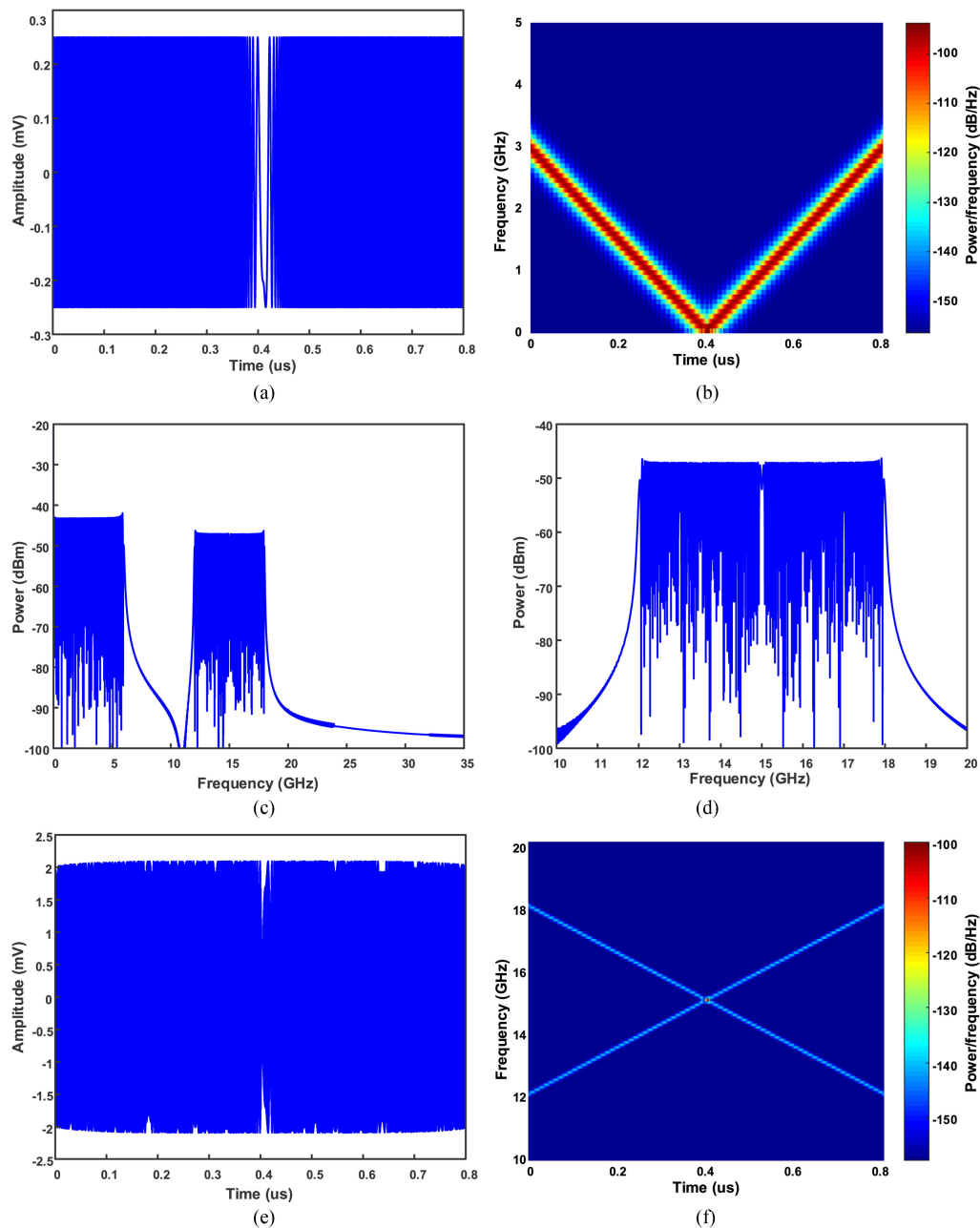
Fig. 2. Simulation results, (a) waveform of the input baseband signal, (b) frequency-time diagram of the input baseband signal, (c) output spectrum from PD, (d) output spectrum from HPF, (e) waveform of the generated dual-chirp microwave signal, (f) frequency-time diagram of the generated dual-chirp microwave signal.

RF signal from a microwave source (ROHDE&SCHWARZ SMB 100A) via an electronic 90° hybrid (ABACUS MICROWAVE 9-010180, 1-18 GHz). The frequency of the applied single-tone RF signal is set to be 1.5 GHz. A 20-Gbps PD (Agilent 11982A) is employed to achieve heterodyne detection of the two optical signals, where the spectrum and the waveform of the output RF signal from the PD are measured by an electronic spectrum analyzer (ROHDE&SCHWARZ FSU50) and a real-time oscilloscope (ROHDE&SCHWARZ RTO 1024), respectively.
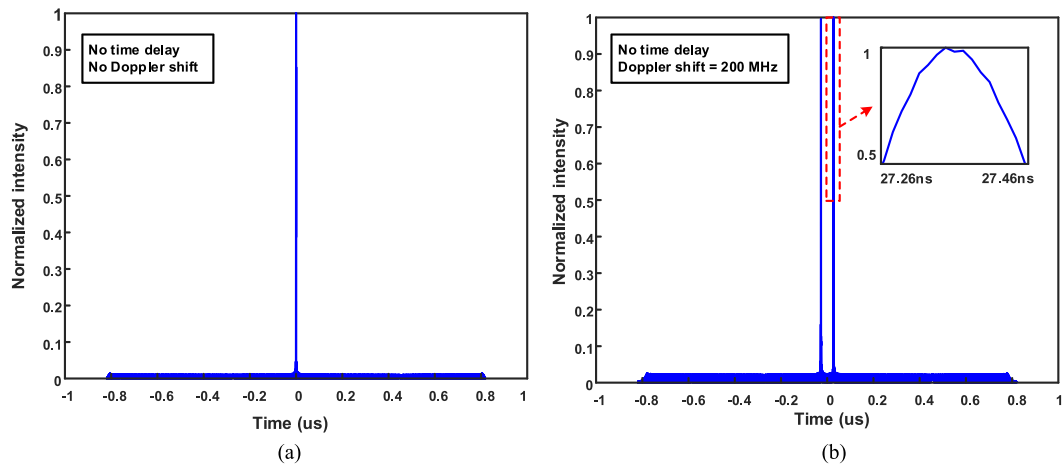
Fig. 3. Matched filtering results of the dual-chirp microwave signal (a) without a Doppler frequency shift, and (b) with a Doppler frequency shift of 200 MHz (inset: the zoom in on half of maximum).

Firstly, a dual-chirp microwave signal with a central frequency of 1.5 GHz, a bandwidth of 100 MHz, a period of 31.25 μs and a duty ratio of 50% is generated. Fig. 4(a) and (b) show the waveform and the frequency-time diagram of the input baseband symmetric-triangle linear frequency modulated signal in a single period, where the peak-to-peak voltage is 5 V, the period is 31.25 μs, the duty ratio is 50%, and the frequency range is from DC to 50 MHz. It can be seen from Fig. 4(b) that, except for the baseband symmetric-triangle LFM signal (the red part), there are spurious components (the green part). These spurious components are attributed to the poor performance of the programmable AWG employed in the experiment, which are detrimental to the dual-chirp microwave signal generation. Fig. 4(c) and (d) present the waveform and the spectrum of the generated signal from the PD, respectively. A digital 4th-order Butterworth HPF with a cut-off frequency of 0.9 GHz is used to filter out the generated baseband signal. Fig. 4(e) and (f) exhibit the waveform and the frequency-time diagram of the signal after filtering, respectively. It can be seen from Fig. 4(f) that the expected dual-chirp microwave signal with a central frequency of 1.5 GHz and a bandwidth of 100 MHz is generated. However, there are two spurious components in the filtered signal, which do not appear in the simulation result as shown in Fig. 2(f). The first one is a single-tone microwave signal with a frequency of 1.5 GHz, which is attributed to the beating between the modulation sideband from the DPMZM and the vestigial carrier from the DPMZM and the MZM. The second spurious component is a dual-chirp microwave signal with a central frequency of 1.5 GHz and a bandwidth of 200 MHz, which is attributed to the 2nd-order modulation sidebands of the MZM. In addition, it should be pointed out that the power of the high-frequency components is smaller than that of the low-frequency components, which is attributed to the narrow bandwidth of the oscilloscope employed in the experiment. The oscilloscope is with a nominal analog bandwidth of 2 GHz, but its response decreases sharply beyond 1.5 GHz. Fig. 4(g) shows the pulse compression result of the generated dual-chirp microwave signal after matched filtering, where the FWHM of the compressed pulse is about 12 ns and the compression ratio is about 1302 (the corresponding TBWP is 1562.5).

Then, the flexibility of the proposed scheme is investigated, where a dual-chirp microwave signal with a central frequency of 1.5 GHz, a bandwidth of 200 MHz, a period of 62.5 μs and a duty ratio of 50% is generated. Fig. 5(a) and (b) show the waveform and the frequency-time diagram of the input baseband symmetric-triangle linear frequency modulated signal in a single period, where the peak-to-peak voltage is 3 V, the period is 62.5 μs, the duty ratio is 50%, and the frequency range is from DC to 100 MHz. It can be also seen from Fig. 5(b) that, except for the baseband
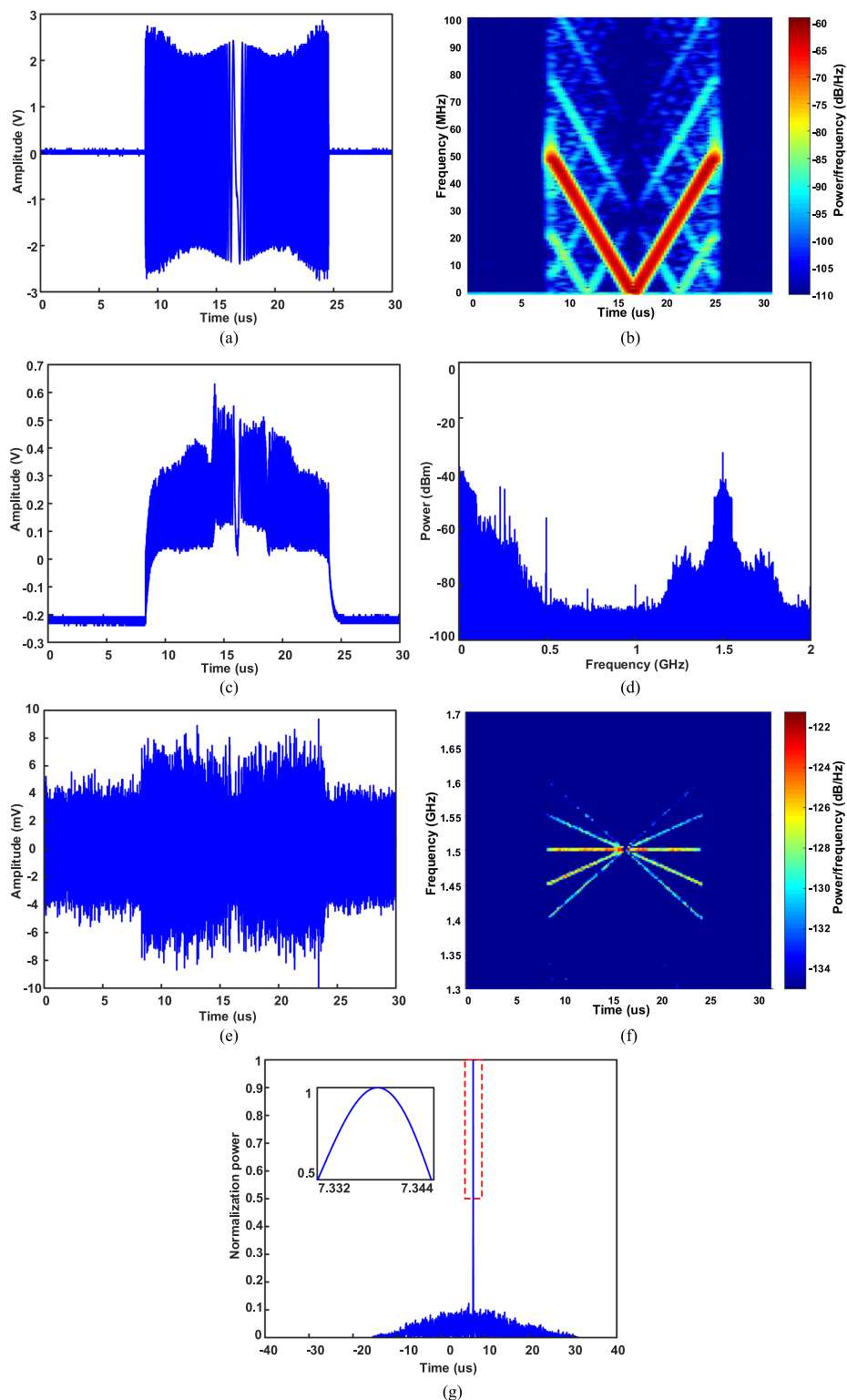
Fig. 4. Experimental results of generating a dual-chirp microwave signal with a bandwidth of 100 MHz, (a) waveform of the input baseband signal, (b) frequency-time diagram of the input baseband signal, (c) waveform from the PD, (d) spectrum from the PD, (e) waveform after digital filtering, (f) frequency-time diagram after digital filtering, (g) pulse compression result of the generated dual-chirp microwave signal after matched filtering (Inset: the zoom in on half of maximum).
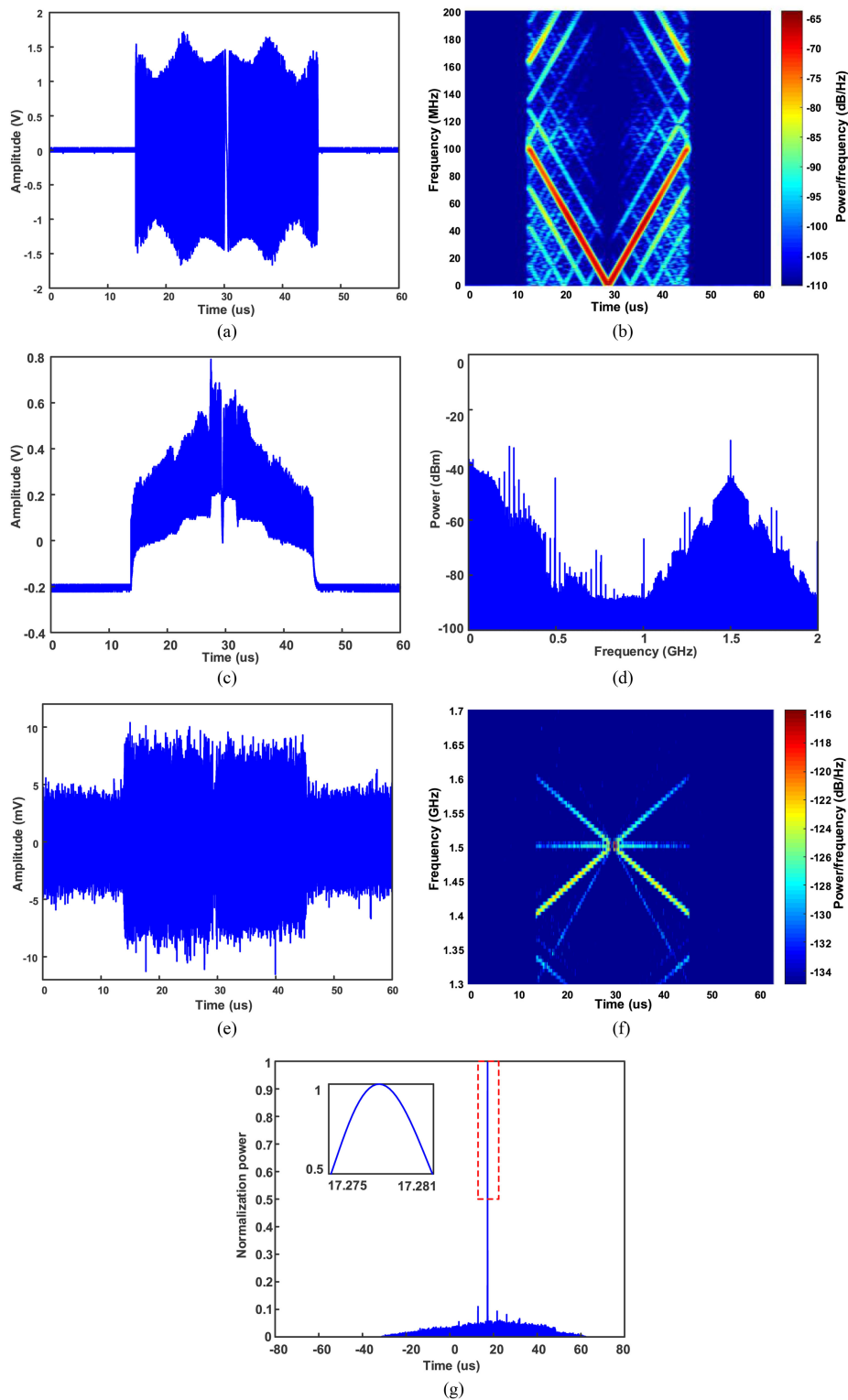
Fig. 5. Experimental results of generating a dual-chirp microwave signal with a bandwidth of 200 MHz, (a) waveform of the input baseband signal, (b) frequency-time diagram of the input baseband signal, (c) waveform from the PD, (d) spectrum from the PD, (e) waveform after digital filtering, (f) frequency-time diagram after digital filtering, (g) pulse compression result of the generated dual-chirp microwave signal after matched filtering (Inset: the zoom in on half of maximum).

symmetric-triangle LFM signal (the red part), there are unwanted spurious components (the green part).

Fig. 5(c) and (d) present the waveform and the spectrum of the generated signal from the PD, respectively. A digital 4th-order Butterworth HPF with a cut-off frequency of 0.9 GHz is also used to filter out the generated baseband signal. Fig. 5(e) and (f) exhibit the waveform and the frequency-time diagram of the signal after filtering, respectively. It can be seen from Fig. 5(f) that the generated dual-chirp microwave signal involves an up-chirped waveform and a down-chirped one in the frequency range of 1.4 GHz to 1.6 GHz. In addition, the unexpected dual-chirp microwave signal with a central frequency of 1.5 GHz and a bandwidth of 400 MHz is negligible since the 2nd-order modulation sidebands of the MZM is suppressed due to the relatively small voltage applied to the MZM. However, the single-tone microwave signal with a frequency of 1.5 GHz still exists. Fig. 5(g) shows the pulse compression result of the generated dual-chirp microwave signal after matched filtering, where the FWHM of the compressed pulse is about 6 ns and the compression ratio is about 5208 (the corresponding TBWP is 6250).

It should be noted that only dual-chirp microwave signals centered at 1.5 GHz are generated in the experiment, which is mainly attributed to the limited test capacity of the employed real-time oscilloscope (with a nominal analog bandwidth of 2 GHz and a sampling rate of 10 GS/s). In fact, the central frequency can reach 18 GHz by using the existing experimental setup, and can be further enhanced to 40 GHz via replacing the 90° hybrid used in the experiment with a broadband one (e.g., Marki QH-0440, 4-40 GHz), together with the employment of a high-speed PD. In addition, the bandwidth of the generated dual-chirp microwave signal is limited by the available bandwidth of the baseband symmetric-triangle linear frequency modulated signal, which can reach multi-GHz or even beyond 10 GHz through replacing the AWG used in the experiment with a high-speed DDS (e.g., ADI AD9162, 12 GS/s).

Finally, it should be pointed out that the spurious single-tone component in the generated signal is mainly attributed to the vestigial carrier in the carrier-suppressed modulation. In order to improve the carrier suppression ratio, a DPMZM can be employed to achieve CS-DSB modulation instead of an MZM. Furthermore, a single dual-polarization QPSK modulator followed by a polarizer can be used to replace the Mach-Zehnder interferometer structure in Fig. 1 to simplify the system architecture and improve the stability.

5. Conclusion

In summary, we have proposed and demonstrated a photonics-assisted approach to generating bandwidth-doubling dual-chirp microwave signals with freely-tunable central frequency based on electro-optic modulation and heterodyne detection. The kernel of the approach is firstly loading a baseband symmetric-triangle linear frequency modulated signal onto the optical carrier via CS-DSB modulation, and then beating the generated dual-chirp optical waveform with a frequency-shifted optical carrier obtained through electro-optic frequency shifting. After heterodyne detection, a dual-chirp microwave signal is generated, where its bandwidth is twice of that of the input baseband signal, and its central frequency is equal to the frequency of the single-tone RF signal. The proposed scheme has been demonstrated by both numerical simulation and experiment. In the simulation, a dual-chirp microwave signal with a central frequency of 15 GHz and a bandwidth of 6 GHz was generated, where the bandwidth of the input baseband symmetric-triangle linear frequency modulated signal was 3 GHz. In the experiment, dual-chirp microwave signals centered at 1.5 GHz and with bandwidth of 100 MHz and 200 MHz were generated, where the pulse compression ratios are 1302 and 5208, respectively. The proposed scheme has the ability to generate dual-chirp microwave signals with flexible tunability of bandwidth, central frequency and duration.

References

[1] M. A. Richards, *Fundamentals of Radar Signal Processing*, 2nd ed.. New York, NY, USA: McGraw-Hill, 2014.

[2] M. I. Skolnik, *Introduction to radar systems*, 2nd ed.. New York, NY, USA: McGraw-Hill, 1980.

[3] R. J. Fitzgerald, "Effects of range-doppler coupling on chirp radar tracking accuracy," *IEEE Trans. Aerosp. Electron. Syst.*, vol. AES-10, no. 4, pp. 528–532, Jul. 1974.

[4] A. Amar and Y. Buchris, "Asynchronous transmitter position and velocity estimation using a dual linear chirp," *IEEE Signal Process. Lett.*, vol. 21, no. 9, pp. 1078–1082, Sep. 2014.

[5] K. Iwashita, T. Moriya, N. Tagawa, and M. Yoshizawa, "Doppler measurement using a pair of FM-chirp signals," in *Proc. IEEE Symp. Ultrason.*, Honolulu, HI, USA, Oct. 2003, pp. 1219–1222.

[6] S. T. Cundiff and A. M. Weiner, "Optical arbitrary waveform generation," *Nature Photon.*, vol. 4, pp. 760–766, Oct. 2010.

[7] R. J. C. Middleton, D. G. Macfarlane, and D. A. Robertson, "Range autofocus for linearly frequency-modulated continuous wave radar," *IET Radar Sonar Navig.*, vol. 5, pp. 288–295, Mar. 2011.

[8] J. Capmany and D. Novak, "Microwave photonics combines two worlds," *Nature Photon.*, vol. 1, pp. 319–330, Jun. 2007.

[9] J. P. Yao, "Microwave photonics," *J. Lightw. Technol.*, vol. 27, no. 3, pp. 314–335, Feb. 2009.

[10] D. Zhu and J. P. Yao, "Dual-chirp microwave waveform generation using a dual-parallel Mach–Zehnder modulator," *IEEE Photon. Technol. Lett.*, vol. 27, no. 13, pp. 1410–1413, Jul. 2015.

[11] Y. X. Xu, T. Jin, H. Chi, S. L. Zheng, X. F. Jin, and X. M. Zhang, "Photonic generation of dual-chirp waveforms with improved time-bandwidth product," *IEEE Photon. Technol. Lett.*, vol. 29, no. 15, pp. 1253–1256, Aug. 2017.

[12] R. Kumar and S. K. Raghuwanshi, "A photonic scheme for the generation of dual linear chirp microwave waveform based on the external modulation technique and its airborne application," *Opt. Quant. Electron.*, vol. 49, pp. 370.1–370.13, Oct. 2017.

[13] S. Zhu, M. Li, N. H. Zhu, and W. Li, "Chromatic-dispersion-induced power-fading suppression technique for bandwidth-quadrupling dual-chirp microwave signals over fiber transmission," *Opt. Lett.*, vol. 44, no. 4, pp. 923–926, Feb. 2019.

[14] X. Li, S. H. Zhao, Z. H. Zhu, K. Qu, T. Lin, and D. P. Hu, "Photonic Generation of Frequency and Bandwidth Multiplying Dual-Chirp Microwave Waveform," *IEEE Photon. J.*, vol. 9, no. 3, Jun. 2017, Art. no. 7104014.

[15] K. Zhang *et al.*, "Photonic approach to dual-band dual-chirp microwave waveform generation with multiplying central frequency and bandwidth," *Opt. Commun.*, vol. 437, pp. 17–26, Apr. 2019.

[16] S. Zhu, M. Li, N. H. Zhu, and W. Li, "Transmission of dual-chirp microwave waveform over fiber with compensation of dispersion induced power fading," *Opt. Lett.*, vol. 43, no. 11, pp. 2466–2469, Jun. 2018.

[17] K. Zhang, S. H. Zhao, T. Lin, X. Li, W. Jiang, and G. D. Wang, "Photonic generation of multi-frequency dual-chirp microwave waveform with multiplying bandwidth," *Opt. Commun.*, vol. 13, Jun. 2019, Art. no. 102226.

[18] T. F. Hao, J. Tang, N. N. Shi, W. Li, N. H. Zhu, and M. Li, "Dual-chirp Fourier domain mode-locked optoelectronic oscillator," *Opt. Lett.*, vol. 44, no. 8, pp. 1912–1915, Apr. 2019.

[19] H. Z. Zhou *et al.*, "Broadband two-thirds photonic microwave frequency divider," *Electron. Lett.*, vol. 55, pp. 1141–1143, Oct. 2019.

[20] T. F. Hao *et al.*, "Breaking the limitation of mode building time in an optoelectronic oscillator," *Nature Commun.*, vol. 9, May 2018, Art. no. 1839.